

Article

Microstructure and Properties of Thermal Electrode Material $\text{Si}_3\text{N}_4\text{-MoSi}_2$ Composite Ceramics

Lichao Feng ^{1,2,*}, Pengfei Guan ¹, Xuemei Yu ^{1,2} and Yiqiang He ¹

¹ School of Mechanical and Ocean Engineering, Huaihai Institute of Technology, Lianyungang 222005, China; gpf543210@163.com (P.G.); yuxuemei_hit@126.com (X.Y.); gali_hit@126.com (Y.H.)

² Marine Resources Development Institute of Jiangsu, Lianyungang 222001, China

* Correspondence: fenglchhit@hhit.edu.cn; Tel.: +86-518-85895330; Fax: +86-518-85895326

Received: 11 May 2018; Accepted: 9 June 2018; Published: 11 June 2018



Abstract: With good high temperature and corrosive resistance performance, ceramic based composites can be used as promising materials to replace metal thermocouple materials. In this study, $\text{Si}_3\text{N}_4\text{-MoSi}_2$ composites were prepared via hot pressing technology. X-ray diffraction (XRD), optical microscopy (OM), and scanning electron microscopy (SEM) were used to analyze the microstructure of the composites. The mechanical properties and electrical conductivity were tested. The results showed that the composites were composed of $\beta\text{-Si}_3\text{N}_4$, MoSi_2 , a small amount of Mo_5Si_3 , and an amorphous glassy phase. The MoSi_2 phase was evenly distributed in the matrix. The percolation network was formed with increasing MoSi_2 content. The strength of the composites reached its maximum value when the MoSi_2 content reached a critical point. The electrical conductivity behaved like a typical percolation phenomenon. The percolation threshold was about 30% to 45%.

Keywords: thermal electrode materials; hot pressing; microstructure; mechanical properties; electrical conductivity

1. Introduction

The thermocouple is the most widely used temperature testing device in many industrial areas [1–3]. To realize accurate temperature testing in a high temperature and corrosive environment, a corrosive and high temperature resistance tube has to be used to protect the metallic thermocouple material [4–8]. However, the application of the protection tube will reduce the stability and accuracy of the thermocouples due to the change of thermo-electrical potential resulting from the variation of the physical status of the metal electrode materials.

With increasing requirements from metallurgy, chemical, and aerospace engineering, the stable properties of thermocouple materials, which can be used in high temperature and corrosive environments, is still a big challenge in materials science, especially when they are used in molten salt electrolysis as the temperature testing device. Apart from the temperature range, the testing accuracy is another important factor that needs to be considered. As a result, a traditional metallic thermocouple is not able to satisfy the requirements when they are exposed to the above-mentioned working environments. Based on this condition, ceramic based composites, which have good high temperature and corrosive resistance performance, have been used as candidate materials to replace metallic thermocouple materials [9–13].

Disordered ceramic composites are composed of at least two types of ceramics, which combines the advantages of each component. Previous studies have demonstrated that $\text{Si}_3\text{N}_4\text{-MoSi}_2$ composites have good mechanical, anti-oxidation, and corrosive resistance performances [14–18]. As a result, they are able to be used as candidate materials to fabricate thermocouple electrode materials. In this study, the mechanical and electrical properties and microstructure of $\text{Si}_3\text{N}_4\text{-MoSi}_2$ composites were

tested and analyzed to shed light on their potential application as new high temperature and corrosive resistance thermocouple materials.

2. Experimental

The Si_3N_4 powders were provided by Shinuorui Co. Ltd., Fuzhou, China and the MoSi_2 powder was provided by Yantai Torch Special High Temperature Ceramics Co. Ltd., Yantai, China. The chemical contents are listed in Table 1, and the microstructures are depicted in Figure 1. All materials were used as received without further purification.

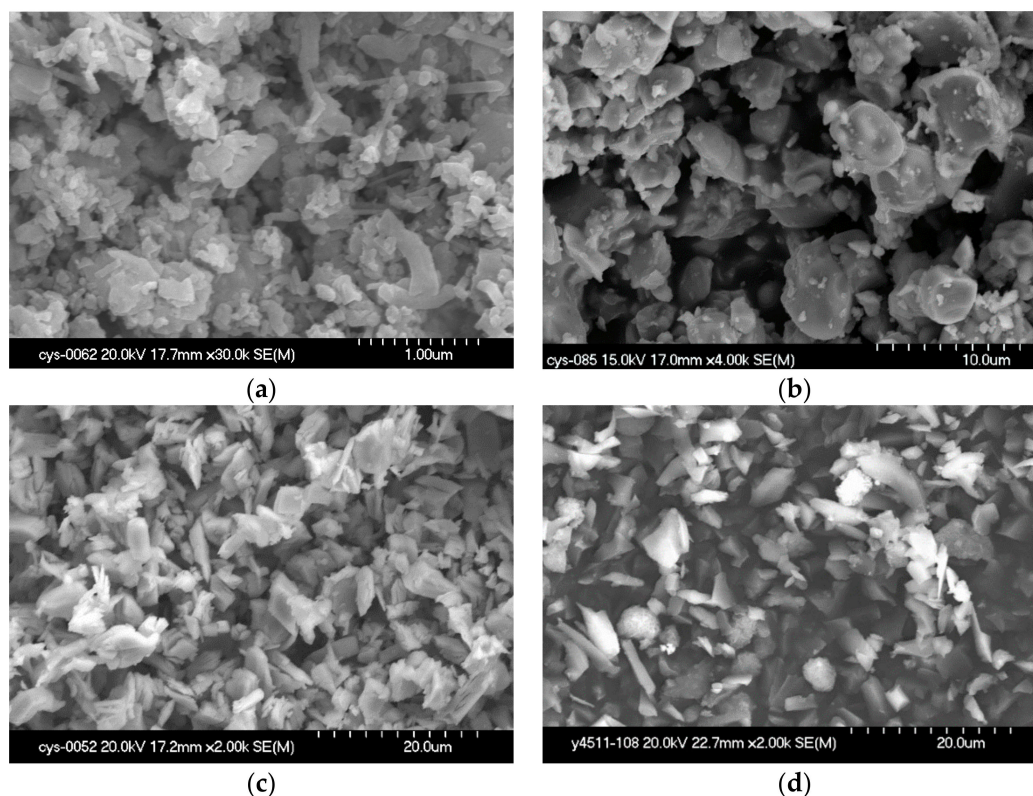


Figure 1. The SEM morphologies of the original powders. (a) $\alpha\text{-Si}_3\text{N}_4$; (b) MoSi_2 ; (c) Y_2O_3 ; (d) La_2O_3 .

Table 1. Chemical contents of the original powders.

α Phase- Si_3N_4 /wt %		MoSi_2 /wt %		La_2O_3 /wt %		Y_2O_3 /wt %	
purity	>92	purity	>99	purity	>99	purity	>99
N	>38.5	Si	>36.5	REO	>94.5	REO	>94.5
O	<1.5	O	<0.85	CaO	<0.15	CaO	<0.15
C	<0.1	Fe	<0.09	Fe_2O_3	<0.10	Fe_2O_3	<0.10
Fe	<200 ppm	C	<0.01	CeO_2	<0.05	CeO_2	<0.05

As can be seen from the chemical contents and microstructures, the purity of the $\alpha\text{-Si}_3\text{N}_4$ was higher than 92% with an average size of 1 μm . The purity of La_2O_3 , and MoSi_2 was higher than 99% with size of 10 μm , and the purity of Y_2O_3 was higher than 99% with an average size of 15 μm , as shown in Table 1.

As listed in Table 2, the contents of MoSi_2 were 30 wt %, 45 wt %, and 60 wt %, with 5 wt % of La_2O_3 , 5 wt % of Y_2O_3 and the rest of Si_3N_4 . Before the hot pressing process, the powders were ball-milled in dehydrated ethyl alcohol for 10 h, and subsequently dried in a vacuum furnace at 100 $^\circ\text{C}$. After drying, the temperature was raised to 1750 $^\circ\text{C}$ with a heating rate of 30 $^\circ\text{C}/\text{min}$, followed by

hot pressing with 25 MPa and a 60 min soak in a graphite mold. The furnace chamber was purged with 0.5 atm of argon gas from the start of the hot pressing procedure. The relative densities of the prepared samples were tested according to the Archimedes method. The flexural strengths were tested through a three point bending method in a universal testing machine (Instron-5569, Instron, Norwood, CO, USA). The size of the samples were $3 \times 4 \times 36 \text{ mm}^3$, and the flexural strength were calculated according to the following equation:

$$\sigma = \frac{3FL}{2bh^2} \quad (1)$$

where F is the fracture loading; L is the space between the two points; and b and h are the width and thickness of the samples, respectively. The loading rate was 0.5 mm/min. The final results were the arithmetic average value of three samples. Before testing, the surfaces of the samples were polished to avoid stress concentration.

Table 2. Constituents of samples.

No.	Si ₃ N ₄ /wt %	MoSi ₂ /wt %	La ₂ O ₃ /wt %	Y ₂ O ₃ /wt %
#1	60	30	5	5
#2	45	45	5	5
#3	30	60	5	5

Thermal shock resistance is one of the most important properties of ceramic materials. It reflects the fracture resistance of a material with exposure to sharp temperature change conditions. In general, the thermal shock resistance can be characterized by the strength remaining rate after thermal shock testing, expressed as [19]:

$$\eta_{rem} = \sigma_T / \sigma_0 \times 100\% \quad (2)$$

where η_{rem} is the flexural strength remaining rate; σ_T is the flexural strength of the material experienced n time thermal shocking at temperature T ; and σ_0 is the original flexural strength. The samples for the remaining strength tests were air cooled at various temperatures 10 times. The final results were the arithmetic average value of three samples.

The phase structures were determined by X-ray diffraction pattern (XRD) on a Rigaku D/max-rA X-ray diffractometer with Cu K α radiation ($\lambda = 1.5406 \text{ \AA}$) (Rigaku Corporation, Tokyo, Japan). The surface morphologies of the samples were observed by scanning electron microscopy with energy dispersive spectroscopy (SEM/EDS), performed on a Hitachi S-4700 scanning electron microscope (Hitachi Corporation, Tokyo, Japan). After that, the cross sectional optical microscopy was observed on Zeiss-MC80-DX (Zeiss, Oberkochen, Germany).

3. Results and Discussion

3.1. XRD Results and Optical Microstructure

Figure 2 shows the XRD pattern of the Si₃N₄-MoSi₂ composites. As demonstrated in this figure, the composites after hot compressing were mainly composed of the β -Si₃N₄ and MoSi₂ phase. Neither Y nor La compounds were detected. Based on this result, it can be claimed that during the hot pressing process, the original α -Si₃N₄ changed to β -Si₃N₄, the sintering additives, Y₂O₃ and La₂O₃, reacted with the Si and O₂ content and formed an amorphous glassy phase. In addition, small amounts of the Mo₅Si₃ phase could also be detected.

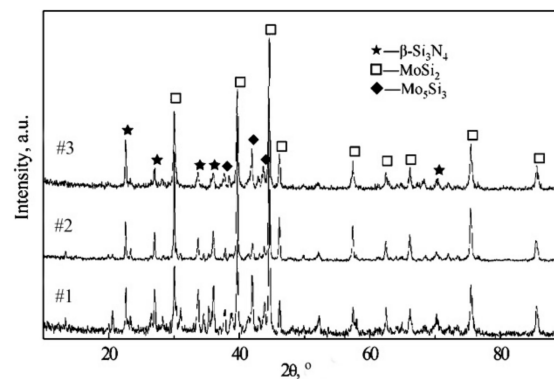


Figure 2. XRD pattern of the Si_3N_4 – MoSi_2 composites.

The densities of the prepared samples are shown in Figure 3. As demonstrated in this figure, the densities of Si_3N_4 -30 wt % MoSi_2 , Si_3N_4 -45 wt % MoSi_2 , and Si_3N_4 -60 wt % MoSi_2 were 4.66 g/cm^3 , 4.31 g/cm^3 , and 3.99 g/cm^3 , respectively. After calculation, the relative densities of the samples were 93.5%, 94.9%, and 95.7%. As can be seen from these results, the samples were all well sintered with a relatively low porosity of less than 6.5%. Previous studies have demonstrated that the densification of Si_3N_4 – MoSi_2 composites is still a challenge without sintering additives [20–23]. It was found that with the addition of Y and La, the densification could be significantly improved [24,25]. Figures 4 and 5 show the optical microscopy, backscattering SEM (BSE), and transmission electron microscopy (TEM) images of Si_3N_4 -30 wt % MoSi_2 , Si_3N_4 -45 wt % MoSi_2 , and Si_3N_4 -60 wt % MoSi_2 , respectively. In the OM and BSE, the white areas are the MoSi_2 phase and the dark areas are the Si_3N_4 phase. As can be seen in these figures, these two phases were evenly distributed, and the interfaces between the two components were clear and smooth. Little microcracks could be observed. The size of the Si_3N_4 was about 3–8 μm , and the size of the MoSi_2 was about 3–5 μm with a uniaxial shape. In addition, the size of the Si_3N_4 slightly reduced with the increasing weight contents of MoSi_2 .

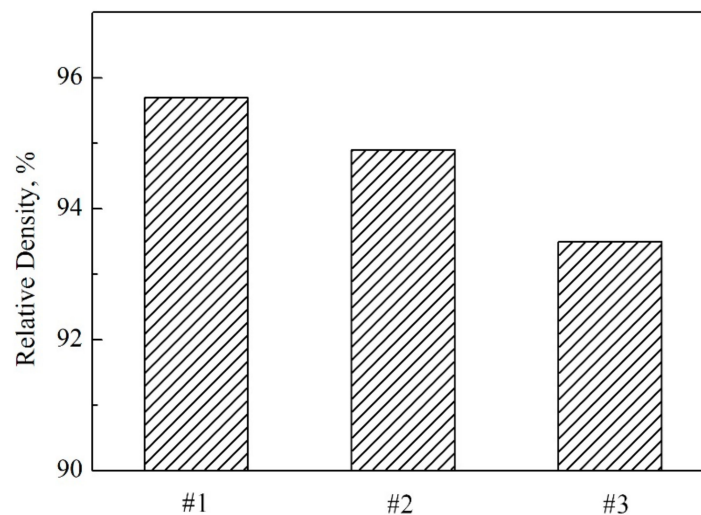


Figure 3. Relative density of the Si_3N_4 – MoSi_2 composites.

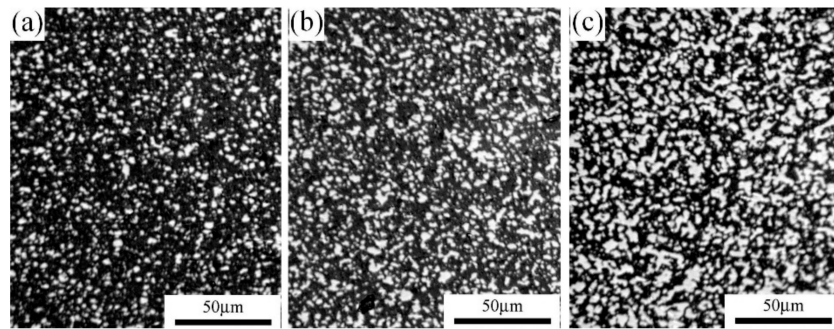


Figure 4. Optical microstructure of the Si_3N_4 - MoSi_2 composites of (a) Si_3N_4 -30 wt % MoSi_2 , (b) Si_3N_4 -45 wt % MoSi_2 , and (c) Si_3N_4 -60 wt % MoSi_2 .

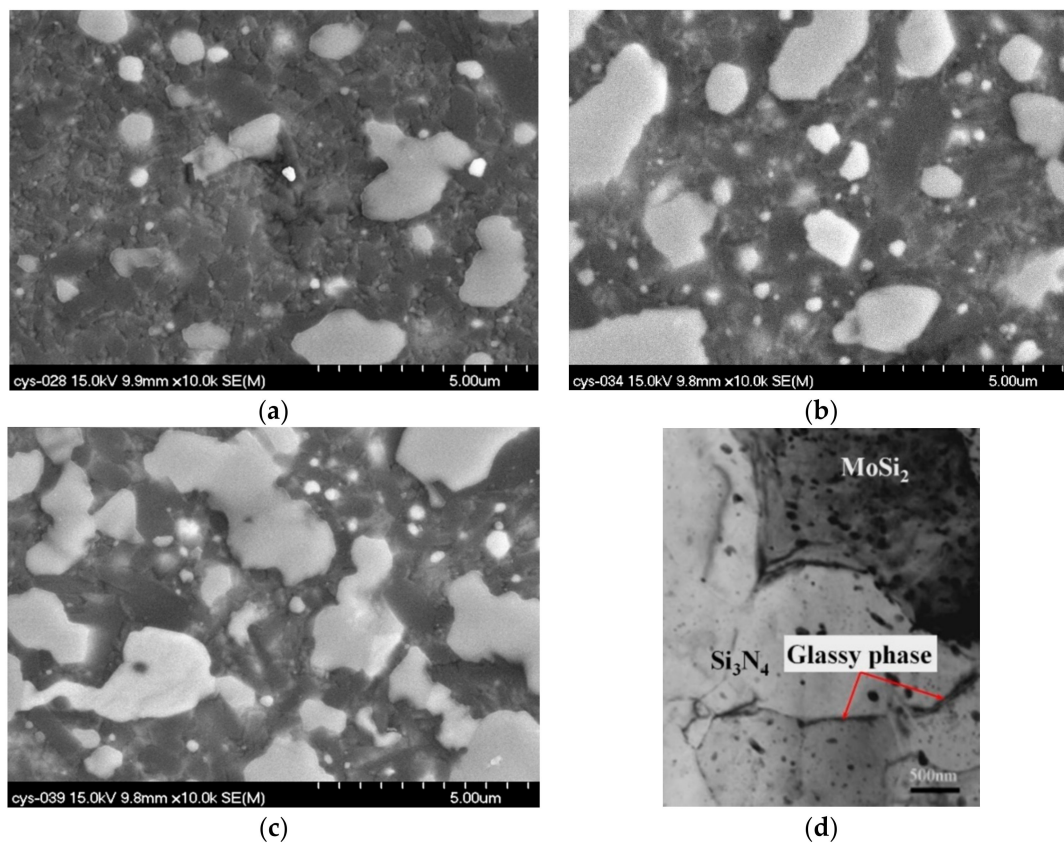


Figure 5. High magnification backscattering SEM of the Si_3N_4 - MoSi_2 composites (a) Si_3N_4 -30 wt % MoSi_2 ; (b) Si_3N_4 -45 wt % MoSi_2 ; (c) Si_3N_4 -60 wt % MoSi_2 , and (d) TEM image.

3.2. Flexural Strength

Figure 6 shows the flexural strengths of the Si_3N_4 - MoSi_2 composites. As illustrated in this figure, the flexural strength of the composites reached 942 MPa, which was higher than that of the pure Si_3N_4 (781 MPa), when the filling content of MoSi_2 reached 30 wt %. However, the flexural strength started to decrease with increasing MoSi_2 content over 30 wt %. The flexural strength decreased to 535 MPa when the MoSi_2 content reached 60 wt %.

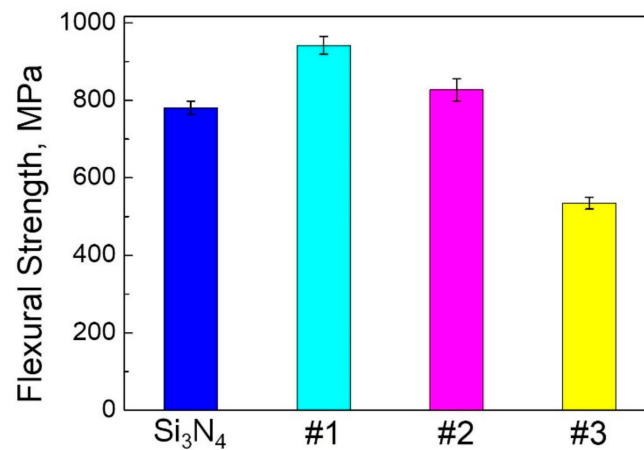


Figure 6. Flexural strengths of the Si₃N₄-MoSi₂ composites.

Figure 7 shows the SEM morphology of the Si₃N₄-MoSi₂ composites. As demonstrated in this figure, the fracture of the composites was a typical inter-granular fracture. The grains of the Si₃N₄ were rod shaped and the grains of MoSi₂ were equiaxial. In sample #1, the grain size of MoSi₂ was relatively small with a size of about 3–5 μm. With an increase of MoSi₂ content, the grain size of MoSi₂ kept increasing slightly, and small amounts of randomly distributed rod shaped Si₃N₄ crystals were observed among the MoSi₂ crystals. It can be concluded that with the addition of MoSi₂, the flexural strength of the composites will start to decrease when the content of MoSi₂ is higher than a critical value due to the increase of porosity and residual stresses.

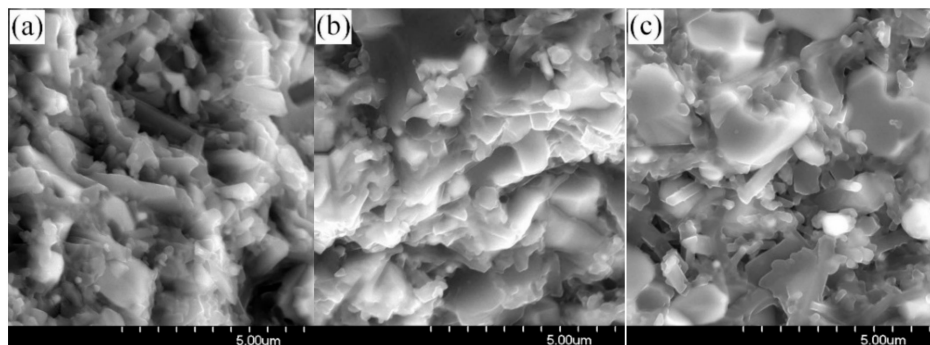


Figure 7. SEM microstructure of the fracture surfaces of Si₃N₄-MoSi₂ composites of sample (a) Si₃N₄-30 wt % MoSi₂; (b) Si₃N₄-45 wt % MoSi₂; (c) Si₃N₄-60 wt % MoSi₂.

3.3. Thermal Shock Resistance

Figure 8 presents the flexural strength remaining rate of the Si₃N₄-MoSi₂ composites at temperatures of 500 °C, 600 °C, and 700 °C after thermal shock testing 10 times. As demonstrated in this figure, the flexural strength remaining rates were 85.2%, 60.5%, and 23.4% corresponding to samples #1, #2, and #3, respectively, when the thermal shock temperature was 500 °C. When the thermal shock testing temperature increased to 600 °C and 700 °C, the flexural strength remaining rate was lower than 20%.

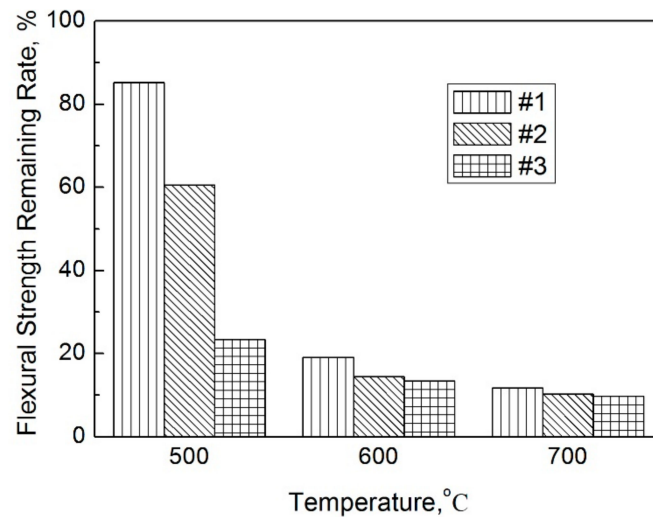


Figure 8. Flexural strength remaining rate of the Si₃N₄-MoSi₂ composites at various temperatures.

Figure 9 shows the SEM microstructure of the fracture surface of sample #1. As demonstrated in this figure, microcracks could be clearly observed when compared with the samples without thermal shock experience. In addition, the quantity and size of the microcracks increased with increasing thermal shock testing temperatures, which resulted from the internal stresses due to the thermal expansion mismatch. As a result, the flexural strengths decreased with the increasing internal stress and thermal mismatch of the two main constituents.

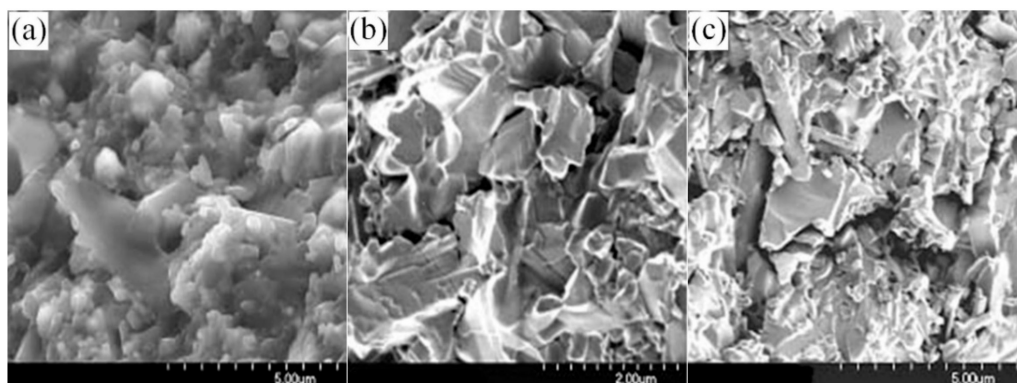


Figure 9. SEM microstructure of the fracture surfaces of the Si₃N₄-MoSi₂ composite samples. (a) Before thermal shock, (b) thermal shock at 500 °C, and (c) thermal shock at 600 °C.

3.4. Electrical Conductivity

Figure 10 illustrates the electrical conductivity of the Si₃N₄-MoSi₂ composites as a function of filling content of MoSi₂. As shown in this figure, the addition of the MoSi₂ could considerably increase the electrical conductivity of the composites. When the content of MoSi₂ reached 30 wt %, the electrical conductivity was $1.25 \times 10^{-5} \Omega^{-1} \cdot \text{m}^{-1}$; when the content increased to 45 wt %, the electrical conductivity increased seven orders of magnitude and reached $3.45 \times 10^2 \Omega^{-1} \cdot \text{m}^{-1}$. After this value, the electrical conductivity increasing rate became flat. This phenomenon can be explained by the percolation theory [13]. Before the percolation threshold, which means that the content of MoSi₂ is relatively low, the MoSi₂ is randomly distributed in the matrix, but no percolation network can be formed. Under this condition, the electrical conductivity is mainly determined by the matrix material, and shows low electrical conductivity. When the MoSi₂ content increased above the percolation threshold, the percolation network of MoSi₂ formed, and as a result, the electrical conductivity

was mainly contributed by the MoSi₂ phase rather than the matrix, thus showing high electrical conductivity. In this study, it can be claimed that the percolation threshold is located between 30 wt % to 45 wt %.

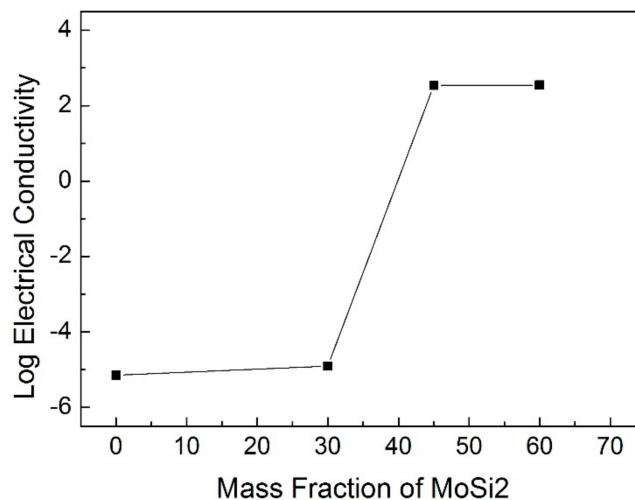


Figure 10. Electrical conductivity of the Si₃N₄-MoSi₂ composites as a function of MoSi₂ mass fraction.

4. Conclusions

In summary, this study successfully prepared Si₃N₄-MoSi₂ composites with hot pressing technology. The main constituents of the hot pressed Si₃N₄-MoSi₂ composites were β-Si₃N₄ and MoSi₂, and a small amount of the Mo₅Si₃ phase and glassy phase containing La and Y. The SEM morphology of the Si₃N₄-MoSi₂ composites demonstrated that the fracture of the composites was a typical inter-granular fracture. The grains of the Si₃N₄ were rod shaped and the grains of MoSi₂ were equiaxial. The strength of the Si₃N₄-MoSi₂ composites decreased with increasing MoSi₂ content. The flexural strength remaining rate of the Si₃N₄-MoSi₂ composites at temperatures of 500 °C, 600 °C, and 700 °C after thermal shocking testing 10 times demonstrated that the flexural strength rates were 85.2%, 60.5%, and 23.4% corresponding to Si₃N₄-30 wt % MoSi₂, Si₃N₄-45 wt % MoSi₂, and Si₃N₄-60 wt % MoSi₂, respectively, when the thermal shock temperature was 500 °C. When the thermal shock testing temperatures increased to 600 °C and 700 °C, the flexural strength remaining rates were lower than 20%.

Author Contributions: L.F. and X.Y. prepared the majority of the manuscript and formatted the references. L.F. provided the main inputs of the manuscript structure and the electrical properties analysis section. P.G. contributed other sections of the properties' analysis. Y.H. provided the microstructure analysis section, the applications section and gave some valuable suggestions on the future studies.

Funding: This work was financially supported by the Natural Science Foundation of the Higher Education Institutions of Jiangsu Province (16KJB430003), the 333 Research Project of Jiangsu Province (BRA2016294), the Lianyungang Scientific Plan-Industrial Program (CG1614), the Lianyungang Scientific Plan-Joint Project of Industry-Academia-Research (CXY1522), the Natural Science Research Project of Huaihai Institute of Technology (Z2017001), and the Six Talent Peaks Program of Jiangsu Province (2013-ZBZZ-032).

Conflicts of Interest: The authors declare no conflict of interest.

References

1. Kerlin, T.W. *Practical Thermocouple Thermometry*; Instrument Society of America: Research Triangle Park, NC, USA, 1999.
2. Hunold, K. Thermocouple for High Temperatures. *Adv. Mater. Process.* **1986**, *2*, 4–5.

3. Farrell, D.M.; Parmar, J.; Robbins, B.J. The Development of Ceramic-Based Thermocouples for Application in Gas Turbines. In Proceedings of the Turbo Expo 2001: ASME Turbo Expo 2001, New Orleans, LA, USA, 4–7 June 2001; pp. 1–5.
4. Klein, R.; Medri, V.; Desmason-Brut, M.; Bellosi, A.; Desmason, J. Influence of Additives Content on the High Temperature Oxidation of Silicon Nitride based Composites. *J. Eur. Ceram. Soc.* **2003**, *23*, 603–611. [[CrossRef](#)]
5. Taguchi, S.P.; Ribeiro, S. Silicon Nitride Oxidation Behaviour at 1000 and 1200 °C. *J. Mater. Process. Technol.* **2004**, *147*, 336–342. [[CrossRef](#)]
6. Cook, J.; Khan, A.; Lee, E.; Mahapatra, M. Oxidation of MoSi₂-based Composites. *Mater. Sci. Eng. A* **1992**, *155*, 183–198. [[CrossRef](#)]
7. Berztiss, D.; Cerchiara, R.R. Oxidation of MoSi₂ and Comparison with Other Silicide Materials. *Mater. Sci. Eng. A* **1992**, *155*, 165–181. [[CrossRef](#)]
8. Tan, W.; Lin, X.P.; Ma, J.T.; Zhang, B.Q. Study on the Conductive Property of Si₃N₄-MoSi₂ Composite Ceramics. *Rare Met. Mater. Eng.* **2011**, *40*, 196–198.
9. Huang, Y.; Lin, J.; Zhang, H. Effect of Si₃N₄ Content on Microstructures and Antioxidant Properties of MoSi₂/Si₃N₄ Composite Coatings on Mo Substrate. *Ceram. Int.* **2015**, *41*, 13903–13907. [[CrossRef](#)]
10. Zhang, H.; Lv, J.; Wu, Y.; Gu, S.; Huang, Y.; Chen, Y. Oxidation Behavior of (Mo, W) Si₂-Si₃N₄ Composite Coating on Molybdenum Substrate at 1600 °C. *Ceram. Int.* **2015**, *41*, 14890–14895. [[CrossRef](#)]
11. Petrovic, J.J. Toughening Strategies for MoSi₂-Based High Temperature Structural Silicides. *Intermetallics* **2000**, *8*, 1175–1182. [[CrossRef](#)]
12. Petrovic, J.J.; Pena, M.I.; Kung, H.H. Fabrication and Microstructures of MoSi₂ Reinforced-Si₃N₄ Matrix Composites. *J. Am. Ceram. Soc.* **1997**, *80*, 1111–1116. [[CrossRef](#)]
13. Kirkpatrick, S. Percolation and Conduction. *Rev. Mod. Phys.* **1973**, *45*, 574–588. [[CrossRef](#)]
14. Balat, M.; Czerniak, M.; Berjoan, R. Oxidation of Silicon Nitride under Standard Air or Microwave-Excited Air at High Temperature and Low Pressure. *J. Mater. Sci.* **1997**, *32*, 1187–1193. [[CrossRef](#)]
15. Sheehan, J.E. Passive and Active Oxidation of Hot-pressed Silicon Nitride Materials with Two Magnesia Contents. *J. Am. Ceram. Soc.* **1982**, *65*, C111–C113. [[CrossRef](#)]
16. Hebsur, M.G. Development and Characterization of SiC(f)/MoSi₂-Si₃N₄(p) Hybrid Composites. *Mater. Sci. Eng. A* **1999**, *216*, 24–37. [[CrossRef](#)]
17. Sadananda, K.; Feng, C.R.; Mitra, R.; Deevi, S.C. Creep and Fatigue Properties of High Temperature Silicides and Their Composites. *Mater. Sci. Eng. A* **1999**, *216*, 223–238. [[CrossRef](#)]
18. Petrovic, J.J.; Pena, M.I.; Reimnis, I.E.; Sandlin, M.S.; Conzone, S.D.; Kung, H.H.; Butt, D.P. Mechanical Behavior of MoSi₂ Reinforced-Si₃N₄ Matrix Composites. *J. Am. Ceram. Soc.* **1997**, *80*, 3070–3076. [[CrossRef](#)]
19. Xie, N.; Shao, W.Z.; Zhen, L.; Feng, L.C. Mechanical and Physical Properties of Cu₂O-xCu Cermet. In *Mechanical Properties and Performance of Engineering Ceramics II: Ceramic Engineering and Science Proceedings*; John Wiley & Sons: Hoboken, NJ, USA, 2007; Volume 27, pp. 423–434.
20. Bundschuh, K.; Schüze, M.; Müller, C.; Greil, P.; Heider, W. Selection of Materials for Use at Temperatures Above 1500 °C in Oxidizing Atmospheres. *J. Eur. Ceram. Soc.* **1998**, *18*, 2389–2391. [[CrossRef](#)]
21. Natesan, K.; Deevi, S.C. Oxidation Behavior of Molybdenum Silicides and Their Composites. *Intermetallics* **2000**, *8*, 1147–1158. [[CrossRef](#)]
22. Kao, M.Y. Properties of Silicon Nitride-Molybdenum Disilicide Particulate Ceramic Composites. *J. Am. Ceram. Soc.* **1993**, *76*, 2879–2883. [[CrossRef](#)]
23. Klemm, H.; Tangermann, K.; Schubert, C.; Hermel, W. Influence of Molybdenum Silicide Additions on High-Temperature Oxidation Resistance of Silicon Nitride Materials. *J. Am. Ceram. Soc.* **1996**, *79*, 2429–2435. [[CrossRef](#)]
24. Schütze, K.B.M. Materials for Temperatures above 1500 °C in Oxidizing Atmospheres Part I: Basic Considerations on Materials Selection. *Mater. Corros.* **2001**, *52*, 204–212.
25. Monteverde, F.; Bellosi, A. High Oxidation Resistance of Hot Pressed Silicon Nitride Containing Yttria and Lanthania. *J. Eur. Ceram. Soc.* **1998**, *18*, 2313–2321. [[CrossRef](#)]

